View metadata, citation and similar papers at core.ac.uk
brought to you by CORE
provided by NASA Technical Reports Server

Temperature Sensing Above 1000ºC Using Cr-Doped $GdAlO_3$ Spin-Allowed Broadband Luminescence

Jeffrey I. Eldridge[a] and Matthew D. Chambers[b]

[a]*NASA Glenn Research Center, Cleveland, OH 44135, USA*
[b]*Raytheon Vision Systems, Goleta, CA 93117, USA*

Abstract. Cr-doped $GdAlO_3$ (Cr:$GdAlO_3$) is shown to produce remarkably high-intensity spin-allowed broadband luminescence with sufficiently long decay times to make effective luminescence-decay-time based temperature measurements above 1000ºC. This phosphor is therefore an attractive alternative to the much lower luminescence intensity rare-earth-doped thermographic phosphors that are typically utilized at these elevated temperatures. In particular, Cr:$GdAlO_3$ will be preferred over rare-earth-doped phosphors, such as Dy:YAG, at temperatures up to 1200ºC for intensity-starved situations when the much lower emission intensity from rare-earth-doped phosphors is insufficient for accurate temperature measurements in the presence of significant radiation background. While transition-metal-doped phosphors such as Cr:Al_2O_3 (ruby) are known to exhibit high luminescence intensity at low dopant concentrations, quenching due to nonradiative decay pathways competing with the ^2E to $^4A_2$ radiative transition (R line) has typically restricted their use for temperature sensing to below 600ºC. Thermal quenching of the broadband $^4T_2$ to $^4A_2$ radiative transition from Cr:$GdAlO_3$, however, is delayed until much higher temperatures (above 1000ºC). This spin-allowed broadband emission persists to high temperatures because the lower-lying ^2E energy level acts as a reservoir to thermally populate the higher shorter-lived $^4T_2$ energy level and because the activation energy for nonradiative crossover relaxation from the $^4T_2$ level to the $^4A_2$ ground state is high. The strong crystal field associated with the tight bonding of the AlO_6 octahedra in the $GdAlO_3$ perovskite structure is responsible for this behavior.

Keywords: Luminescence, phosphor, temperature measurement

INTRODUCTION

Optical temperature measurements using luminescence decay of thermographic phosphors is a well-established technique, and a variety of phosphors with different ranges of temperature sensitivity have been demonstrated that, in combination, cover the temperature range from absolute zero to 1700ºC.[1-4] For making temperature measurements above 1000ºC, thermographic phosphors incorporating rare-earth dopants, such as Dy^{3+}, Tm^{3+}, Tb^{3+} and Eu^{3+}, have been utilized almost exclusively. The 4f electrons in these rare-earth dopants are shielded by the 5s and 5p electrons, resulting in weakly phonon-coupled, spin-forbidden 4f electron transitions. This weak phonon-coupling delays thermal quenching to much higher temperatures compared to transition metal dopants with unshielded 3d electrons. Unfortunately, the oscillator strengths for the 4f transitions are several orders of magnitude weaker than for the 3d transitions,[5] resulting in much lower luminescence emission intensity. This low luminescence emission intensity produced by rare-earth dopants, especially in the presence of the intense background thermal radiation that is common in industrial applications, has been a severe impediment for the successful implementation of thermographic phosphors at temperatures above 1000ºC. The more attractive high luminescence intensity observed from transition-metal-doped phosphors has not been previously achievable for temperature measurements above 1000ºC because strong phonon coupling produces thermal quenching at lower temperatures; for example, temperature measurements using the decay of the luminescence from Cr:Al_2O_3 (ruby) have an upper temperature limit of about 600ºC.[6-13] A secondary drawback to utilizing Cr^{3+} dopant luminescence is that emission occurs at long wavelengths (~700 nm R-line emission) where the background thermal radiation is much more intense at than at the shorter emission wavelengths produced by rare earth dopants selected for high temperature measurements (e.g., 456 nm emission from Dy:YAG).[1,2,14-16]

This paper presents a novel use of the spin-allowed broadband luminescence emission from Cr-doped $GdAlO_3$ (Cr:$GdAlO_3$)[17] that offers the benefit of high luminescence emission intensity typical of a transition metal dopant, but with thermal quenching delayed to the much higher temperatures normally associated with rare-earth dopant luminescence. In addition, the spin-allowed broadband emission extends the range of useful Cr^{3+} luminescence towards shorter wavelengths (<600 nm) where thermal background

radiation is less intense. The Cr:$GdAlO_3$ thermographic phosphor (and closely related phosphors)[17] therefore offers superior performance to rare-earth-doped thermographic phosphors to at least 1200ºC in any situation where the much weaker rare-earth dopant luminescence limits temperature measurement accuracy and reliability.

Rationale for Selection of Cr:$GdAlO_3$

Transition metal dopants are not usually considered for thermographic-phosphor-based temperature measurements above 1000ºC due to the aforementioned thermal quenching at lower temperatures. Furthermore, spin-allowed broadband luminescence emission from transition metal dopants typically exhibits much shorter radiative decay times and stronger thermal quenching than the spin-forbidden R-line emission. However, Zhang et al.[7] have shown that in high-crystal-field Cr^{3+}-doped crystals, the long-lived ^2E energy level can act as a reservoir for the higher lying $^4T_2$ energy level that is responsible for the spin-allowed broadband emission via radiative relaxation to the $^4A_2$ ground state. Fig. 1 shows a single configurational coordinate plot for high-crystal-field (where the $^4T_2$ level is higher in energy than the ^2E level) Cr^{3+}-doped crystals (such as Cr:Al_2O_3 and Cr:$GdAlO_3$), where ΔE is the energy difference between the $^4T_2$ and underlying 2E levels, ΔEq is the energy barrier between the zero-phonon $^4T_2$ state to the $^4T_2$–to-$^4A_2$ crossover by multiphonon absorption, and Δ_{FC} is the Franck-Condon offset between the $^4T_2$ and $^4A_2$ parabolas. At increasing temperatures, thermal equilibrium between the ^2E and $^4T_2$ levels results in an increasing promotion of ions from the much longer-lived ^2E reservoir level to the $^4T_2$ level. Therefore, the spin-allowed broadband radiative relaxation from the $^4T_2$ to $^4A_2$ ground state increases as the emission associated with the spin-forbidden ^2E to $^4A_2$ radiative transition decreases. At even higher temperatures, non-radiative crossover from the $^4T_2$ to $^4A_2$ states increases due to higher phonon population levels and leads to the eventual thermal quenching of the spin-allowed broadband emission. Because thermal equilibrium is maintained between the ^2E and $^4T_2$ populations, the observed decay time of the observed ^2E to $^4A_2$ emission, τ_{2E}, and that of the $^4T_2$ to $^4A_2$ broadband emission, τ_{4T2}, both reflect the depopulation of the ^2E reservoir. Therefore, $\tau_{2E} = \tau_{4T2}$. Zhang et al.[7] showed that the decay time associated with these ^2E reservoir depopulation processes as a function of temperature, T, can be expressed by:

$$\tau_{4T2} = \tau_{2E} = \tau_{2E}^{R} \frac{1+3e^{-\Delta E/kT}}{1+\alpha e^{-\Delta E/kT}+\beta e^{-(\Delta Eq+\Delta E)/kT}} \quad (1)$$

where $1/\tau_{2E}^{R}$ is the intrinsic radiative rate of the ^2E to $^4A_2$ transition, $\alpha = \tau_{2E}^{R}/\tau_{4T2}^{R}$, $\beta = \tau_{2E}^{R}/\tau_q$, $1/\tau_{4T2}^{R}$ is the intrinsic radiative rate of the $^4T_2$ to $^4A_2$ transition, $1/\tau_q$ is a scaling factor for the nonradiative $^4T_2$ to $^4A_2$ crossover rate, and k is Boltzmann's constant. Assuming α and β » 1, this relationship shows that thermal quenching of the observed broadband $^4T_2$ to $^4A_2$ transition can be delayed to higher temperatures by increases in ΔE and in ΔEq. Tanabe-Sugano diagrams for $3d^3$ electron configurations indicate that ΔE increases with the strength of the crystal field.[7,18] Furthermore, ΔEq becomes greater for stronger bonding, since the stronger restoring force on a displaced ion will result in a greater steepening of the $^4T_2$ parabola (which involves bonding orbitals) than the $^4A_2$ parabola (which does not involve bonding orbitals).

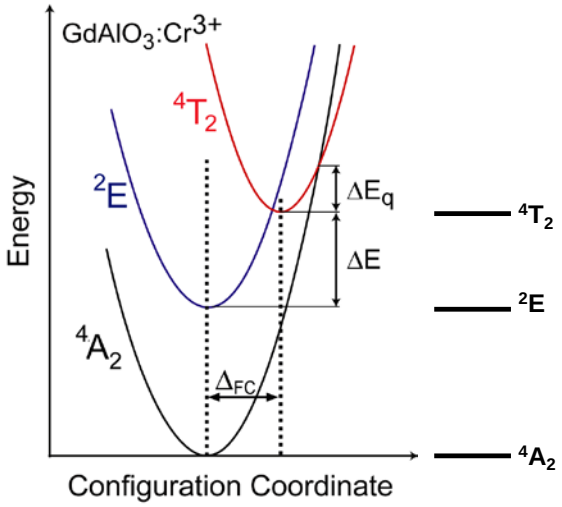

Figure 1. Single configurational coordinate plot (left) and energy level diagram (right) for high-crystal-field Cr^{3+}-doped phosphors such as Cr:$GdAlO_3$.

In view of these considerations, rare-earth aluminate orthorhombic perovskites, $REAlO_3$, are ideal crystal hosts for Cr^{3+} dopants. The Cr^{3+} dopant ions substitute for the Al^{3+} ions in the tightly bound AlO_6 octahedra within the $REAlO_3$ perovskite structure,[19] resulting in exceptionally strong crystal fields (20% higher at Al^{3+} sites in $GdAlO_3$ compared to Al_2O_3).[20] Among the rare-earth aluminate perovskites, $REAlO_3$, only the perovskites with RE = Gd, Tb, Dy, Y, Ho, Er, and Tm retain an orthorhombic perovskite structure from room temperature to above 1000ºC.[21] The others exist in either rhombohedral or cubic structures,[21] with undistorted cubic symmetry at the Al^{3+} sites in the AlO_6 octahedra, and therefore will exhibit undesirably weak excitation transition oscillator strengths. Among

the remaining candidate rare-earths, the crystal field at the Al^{3+} octahedral sites is expected to decrease in the order from largest to smallest ionic radii (Gd>Tb>Dy>Y>Ho>Er>Tm).[21] Therefore, Cr:$GdAlO_3$ is expected to delay thermal quenching of the spin-allowed broadband emission to higher temperatures than the other perovskite candidates. It should be noted that while the spin-forbidden luminescence from the perovskite Cr:$YAlO_3$ for temperature sensing has been previously reported,[22] measurements were only made up to 75ºC and no attempt was made to utilize its spin-allowed broadband emission at shorter wavelengths.

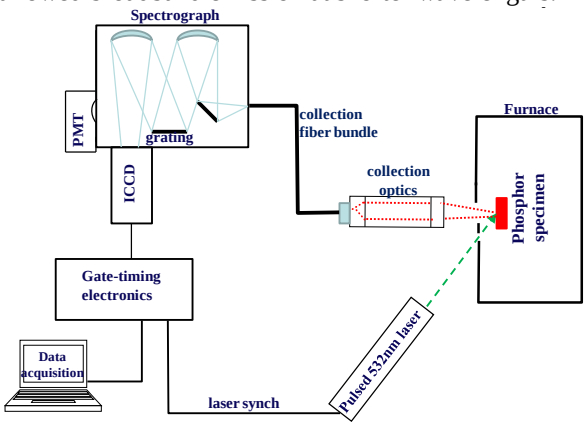

Figure 2. Time-resolved luminescence emission setup.

EXPERIMENT

Specimens were 25.4-mm diameter disks produced by sintering Cr:$GdAlO_3$ powder with a formula of $GdAl_{0.998}Cr_{0.002}O_3$, for a 0.2% Cr^{3+} cation doping level. Time-averaged and time-resolved luminescence emission spectra were collected using the experimental arrangement shown in Fig. 2. The specimen was placed inside a box furnace with two access holes in the back. Excitation by a pulsed 20 Hz, 532 nm (frequency double YAG:Nd) laser was transmitted through one of the access holes while luminescence emission was collected by a collection optics assembly with a 125 mm working distance through the other access hole. Fig. 3 shows an excitation spectrum obtained from a Cr:$GdAlO_3$ specimen, showing the choice of the 532 nm excitation was from a very wide range of excitation wavelengths that could be selected. The collected luminescence emission was transmitted via a fiber optic cable to a spectrograph, where time-resolved spectra were acquired by an intensified CCD (ICCD) camera or time-averaged spectra were acquired by a photomultiplier tube (PMT) through a slit. After an optimum wavelength range was selected, luminescence decay measurements were obtained by replacing the spectrograph with the appropriately selected bandpass filter in front of a PMT.

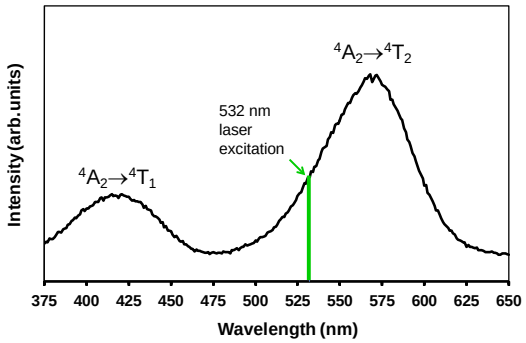

Figure 3. Room temperature excitation spectrum for Cr:$GdAlO_3$. Emission at 728 nm.

RESULTS

Fig. 4 shows the time-averaged luminescence emission spectra of a Cr:$GdAlO_3$ specimen as a function of temperature. It is evident from these spectra that the broadband emission centered at 640 nm becomes more prominent while the spin-forbidden R-line emission at 728 nm and the Stokes phonon-loss peak at 700 nm become less prominent with increasing temperature. It is also apparent that at the highest temperatures (>700ºC), the shorter-wavelength broadband emission dominates the emission spectra and therefore is the only component of luminescence emission remaining that can be used for temperature measurements.

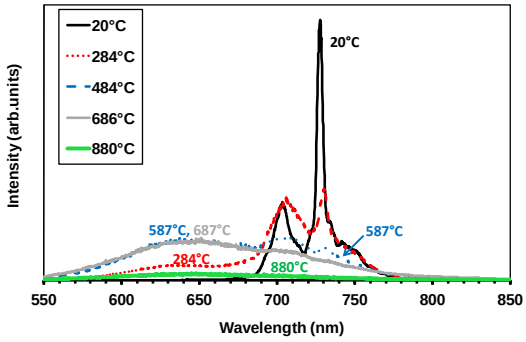

Figure 4. Temperature dependence of luminescence emission spectra for Cr:$GdAlO_3$. Excitation at 532 nm.

Time-resolved luminescence emission spectra at increments of delay after the laser excitation pulse were collected over a temperature range from room temperature to 1072ºC. Examples of series of time-resolved spectra are shown for 378ºC and 1072ºC in Figs. 5-6. Fig. 5a shows the decay of the mixture of sharp R-line emission and broadband emission at 378ºC. The same data is re-presented as a series of decay measurements at different wavelengths with a logarithmic intensity scale in Fig. 5b. The uniform downward slope across the full wavelength range (570-850 nm) in Fig. 5b suggests the same exponential

decay for all wavelengths within this range, i.e. , $\tau_{2E} = \tau_{4T2}$, as expected for thermal equilibrium between the ^2E and $^4T_2$ populations. To provide a more quantitative indication of the decay rate uniformity across the full emission spectra, exponential decay constants were determined by nonlinear regression for six wavelength intervals starting with 570-600 nm and followed by 50-nm-span intervals up to 850 nm. At 378ºC, averaging the determined decay constants from these wavelength intervals gave a mean of 3.85 msec with a standard deviation of ±0.05 msec (corresponds to about ±2ºC). At 1072ºC, the mean of the decay rate was 1.45 µsec with a standard deviation of ±0.11 µsec (corresponds to about ±5ºC). The significance of this uniform decay behavior is that the decay-time/temperature calibration is insensitive to the choice of emission wavelength. This allows considerable flexibility in emission wavelength range selection, which can therefore be determined purely by consideration of signal intensity and avoidance of competing thermal radiation background. Fig. 6a displays the time-resolved spectra acquired at 1072ºC, with only broadband emission remaining at this temperature. Fig. 6b, replotted as a series of decay curves at different wavelengths on a logarithmic intensity scale, shows a uniform luminescence decay rate for the broadband luminescence emission at 1072ºC.

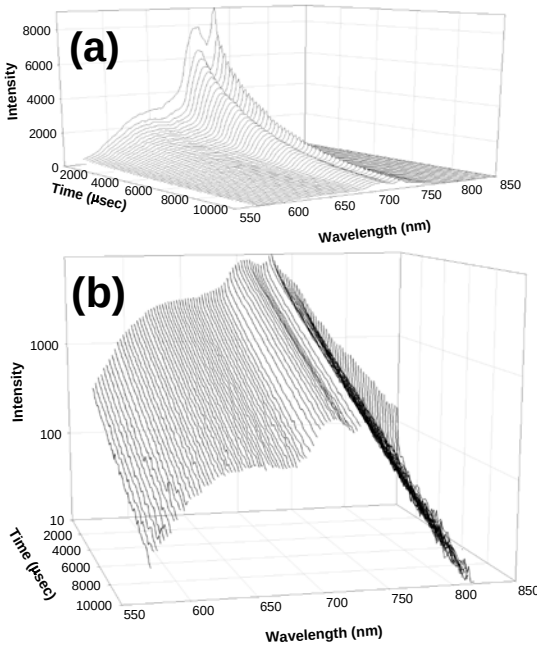

Figure 5. 3D plots showing time-resolved decay of luminescence emission spectra from Cr:$GdAlO_3$ at 378ºC. (a) Linear intensity scale. (b) Logarithmic intensity scale shows uniform slope over full wavelength range, indicating wavelength-independent decay time.

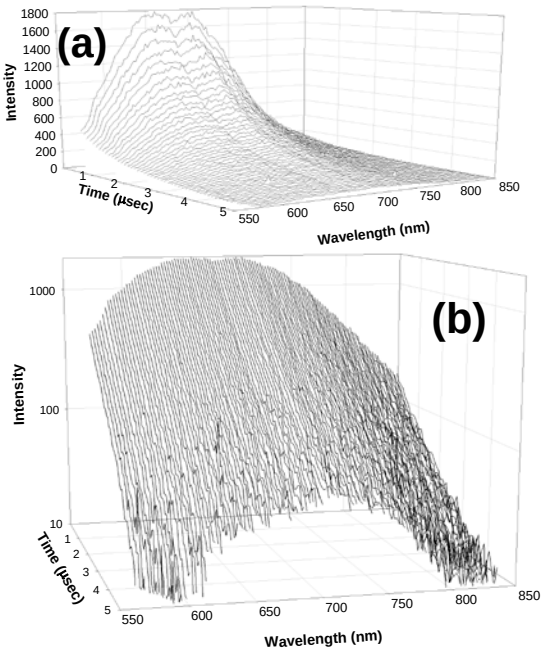

Figure 6. 3D plots showing time-resolved decay of luminescence emission spectra from Cr:$GdAlO_3$ at 1072ºC. (a) Linear intensity scale. Only broadband emission remains. (b) Logarithmic intensity scale shows uniform slope over full wavelength range, indicating wavelength-independent decay time.

Fig. 6b shows that while the signal intensity at the short wavelength end of the range (570 nm) is substantially lower than at the peak intensity at 640 nm, there is still more than adequate signal intensity at 570 nm (where interference by background thermal radiation is much lower) to accurately determine the luminescence decay constant. Because of the wavelength-independent decay behavior, spectral information is unnecessary for obtaining reliable decay constants. Therefore, luminescence decay calibration data were obtained using a PMT with a bandpass filter to take advantage of the much greater light throughput compared to spectrograph acquisition. A bandpass filter centered at 590 nm with a full-width half-max of 40 nm was selected as a good compromise between collecting a wide wavelength range for greater signal while avoiding thermal radiation background at longer wavelengths. Luminescence decay curves acquired at various temperatures up to 1076ºC using this bandpass filter are shown in Fig. 7. Although these decay curves are nearly single exponential, they were fitted by a double exponential equation due to a short, fast initial decay: $I = I_1 e^{-t/\tau_1} + I_2 e^{-t/\tau_2}$, where I is the intensity, t is time, τ_1 is the time constant associated with the short initial decay, and τ_2 is the time constant associated with the dominant long-term decay. The values of τ_2 were used for temperature calibration.

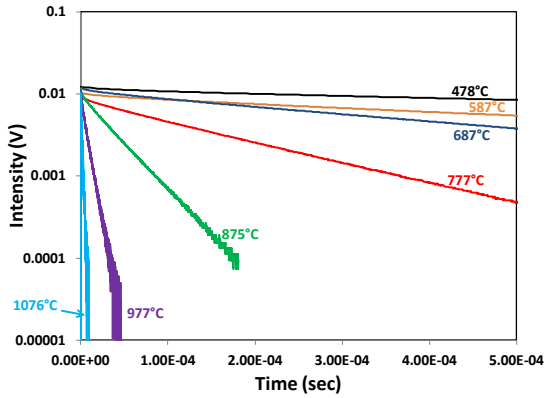

Figure 7. Luminescence decay at various temperatures from $Cr:GdAlO_3$. Using bandpass filter centered at 590 nm with a full-width half-max of 40 nm.

Based on the determined decay constants, a calibration between decay time and temperature up to 1075ºC (the furnace limit) is shown in Fig. 8. These decay time vs. temperature data were in turn fitted by Equation 1, with fitting parameters τ_{2E}^{R}, ΔE, ΔEq, ln(α), and ln(β). The solid line in Fig. 8 is the fit of Equation 1 to the data using the Levenberg-Marquardt nonlinear least squares regression method, where to adequately weight the agreement between the data and the fit for the small decay values (decay values spanned four decades), the residuals were taken as the differences between the natural logarithms of the data and fit values.[2] The parameter values produced by this fit are listed in Table 1. Fig. 8 shows that a short extrapolation of the fit predicts decay times of 1.1 µsec at 1100ºC and 310 nsec at 1200ºC.

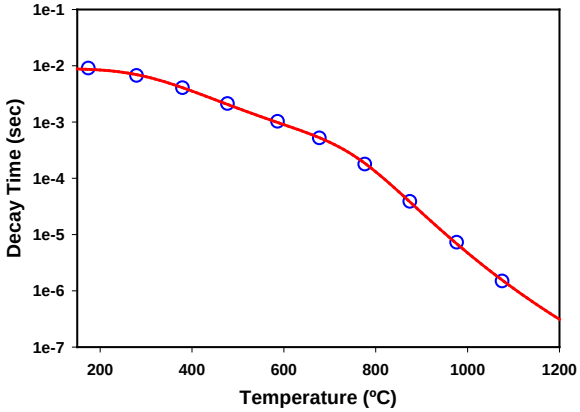

Figure 8. Temperature dependence of $Cr:GdAlO_3$ luminescence decay time for wavelengths selected by bandpass filter centered at 590 nm with a full-width half-max of 40 nm. Circles are values determined from measurements. Solid line is obtained by fitting Equation 1 to the data.

Table 1. Parameters determined by fitting Equation 1 to data in Fig. 8.

τ_{2E}^{R} (msec)	τ_{4T2}^{R} (µsec)	τ_q (sec)	ΔE (cm^{-1})	ΔEq (cm^{-1})
8.90	2.67	5.9×10^{-15}	3600	14525

DISCUSSION

The exceptional persistence of the spin-allowed broadband luminescence from $Cr:GdAlO_3$ to surprisingly high temperatures can be attributed to the strong crystal field the Cr^{3+} dopant ion experiences where it substitutes for the Al^{3+} ions inside the AlO_6 octahedra within the orthorhombic perovskite structure. In particular, the strong crystal field results in both a large ΔE between the $^4T_2$ and underlying ^2E levels and also a large activation barrier, ΔEq, against non-radiative crossover to the $^4A_2$ ground state (Fig. 1). The effects of the large ΔE and ΔEq values are observed in the temperature dependence of the decay behavior shown in Fig. 8, and are effectively modeled by Equation 1. There appear to be two distinct regimes of luminescence decay, as previously reported for $Cr:Al_2O_3$ and other high crystal field hosts.[23,24] The first, more slowly decreasing regime observed in Fig. 8 is from about 200 to 750ºC, and can be attributed to the effect of the thermal population of the $^4T_2$ level at the expense of the ^2E reservoir population. This population shift to the higher $^4T_2$ level occurs with no decrease in radiative efficiency, and the observed decay time decreases because a greater fraction of the radiative decay occurs from the much shorter-lived $^4T_2$ level. One of the beneficial consequences of this shift is that more of the luminescence is produced at the shorter wavelengths associated with the broadband emission where there is less interference from thermal background radiation than for the R-line emission at 728 nm. The second, more steeply decreasing decay regime starts at about 750ºC where the effects of non-radiative crossover from the $^4T_2$ to $^4A_2$ levels become a significant alternate relaxation pathway, reducing both radiative efficiency and decay time. While both these regimes and underlying mechanisms have been described for other Cr-doped phosphors, the higher values of ΔE and ΔEq for $Cr:GdAlO_3$ extend these regimes to much higher temperatures. For example, the estimated value of ΔE for $Cr:GdAlO_3$ is 3600 cm^{-1}, considerably higher than the 2350 cm^{-1} value for $Cr:Al_2O_3$.[7] The higher ΔE delays the thermal depopulation from the ^2E reservoir to higher temperatures. Based on the much higher ΔE value for $Cr:GdAlO_3$, the fraction of excited Cr^{3+} ions that

populate the $^4T_2$ level of $Cr:GdAlO_3$ will be much lower than for $Cr:Al_2O_3$ at the same temperature. Therefore, the equivalent thermal promotion of Cr^{3+} ions to the $^4T_2$ level will be delayed to substantially higher temperatures for $Cr:GdAlO_3$; for example, the fraction of excited Cr^{3+} ions that populate the $^4T_2$ level of $Cr:GdAlO_3$ will not reach the fraction obtained for $Cr:Al_2O_3$ at 600ºC until $Cr:GdAlO_3$ reaches 1060ºC. Similarly, a higher ΔEq delays the thermal quenching by non-radiative crossover to higher temperatures.

In summary, the spin-allowed broad luminescence emission from the $Cr:GdAlO_3$ exhibits considerable advantages for performing luminescence-decay-based temperature measurements up to 1200ºC. Typical of transition metal dopant phosphors, this phosphor offers intense luminescence and a flexible selection of excitation wavelengths, and the utilization of the spin-allowed broadband emission allows for a flexible selection of emission wavelengths. The most novel attribute of this phosphor is the unusual persistence of sufficiently long-lived spin-allowed broadband emission to higher temperatures. Selection of the shorter emission wavelengths associated with the broadband emission provides the additional benefit of reduced interference from interfering thermal radiation background. In particular, $Cr:GdAlO_3$ will be preferred over weaker-intensity rare-earth-doped phosphors, such as Dy:YAG, at temperatures up to 1200ºC for intensity-starved situations when the much lower emission intensity from rare-earth-doped phosphors is insufficient for accurate temperature measurements in the presence of significant radiation background.

ACKNOWLEDGEMENT

We are grateful for the support of the NASA Aeronautics Research Mission Directorate Seedling Fund.

REFERENCES

1. Allison, S. W., and Gillies, G. T., *Rev. Sci. Instrum.* **68**, 2615-2650 (1997).
2. Chambers, M. D., and Clarke, D. R., *Annu. Rev. Mater. Res.* **39**, 325-359 (2009).
3. Aldén, M., Omrane, A., Richter, M., and Särner, G., *Prog. Energy Combust. Sci.* **37**, 422-461 (2011).
4. Heyes, A. L., *J. Lumin.* **129**, 2004-2009 (2009).
5. Vergeer, P., "Experimental Techniques," in *Luminescence: From Theory to Applications* edited by C. Ronda, Weinheim, Wiley-VCH, 2008, pp. 219-250.
6. Grattan, K. T. V., and Zhang, Z. Y., *Fiber Optic Fluorescence Thermometry*, London, Chapman & Hall, 1995.
7. Zhang, Z., Grattan, K. T. V., and Palmer, A. W., *Phys. Rev. B* **48**, 7772-7778 (1993).
8. Shen, Y., Tong, L., Wang, Y., and Ye, L., *Appl. Opt.* **38**, 1139-1143 (1999).
9. Grattan, K. T. V., Zhang, Z. Y., Sun, T., Shen, Y., Tong, L., and Ding, Z., *Meas. Sci. Technol*. **12**, 981-986 (2001).
10. Seat, H. C., Sharp, J. H., Zhang, Z. Y., and Grattan, K. T. V., *Sens. Actuators A* **101**, 24-29 (2002).
11. Seat, H. C., and Sharp, J. H., *IEEE Trans. Instrum. Meas.* **53**, 140-154 (2004).
12. Aizawa, H., Uchiyama, H., Katsumata, T., Komuro, S., Morikawa, T., Ishizawa, H., and Toba, E., *Meas. Sci. Technol.* **15**, 1484-1489 (2004).
13. Atakan, B., Eckert, C., and Pflitsch, C., *Meas. Sci. Technol.* **20**, 1-9 (2009).
14. Feist, J. P., Heyes, A. L., Choy, K. L., and Su, B., "Phosphor Thermometry for High Temperature Gas Turbine Applications," in *International Congress on Instrumentation in Aerospace Simulation Facilities*, ICIASF'99, 1999, pp. 6/1-6/7.
15. Eldridge, J. I., Bencic, T. J., Allison, S. W., and Beshears, D. L., *J. Thermal Spray Technol*. **13**, 44-50 (2004).
16. Särner, G., Richter, M., and Aldén, M., *Meas. Sci. Technol.* **19**, 1-10 (2008).
17. Eldridge, J. I., and Chambers, M. D., utility patent application filed.
18. Henderson, B., and Imbusch, G. F., *Optical Spectroscopy of Inorganic Solids*, Oxford, Clarendon Press, 1989.
19. Blazey, K. W., and Burns, G., *Proc. Phys. Soc*. **91**, 640-644 (1967).
20. Merkle, L., Verdun, H. R., Brauch, U., Fuente, G. F. de la, Behrens, E., Thomas, L. M., and Allik, T. H., *J. Opt. Soc. Am. B* **6**, 2343-2347 (1989).
21. Vasylechko, L., Senyshyn, A., and Bismayer, U., "Perovskite-Type Aluminates and Gallates," in *Handbook on the Physics and Chemistry of Rare Earths, Vol. 39*, edited by K.A. Gschneidner, Jr., J.-C. G. Bünzil, and V.K. Pecharsky,Netherlands:North-Holland, 2009, pp. 113-295.
22. Uchiyama, H., Aizawa, H., Katsumata, T., Komuro, S., and Morikawa, T., *Rev. Sci. Instrum.* **74**, 3883-3885 (2003).
23. Kisliuk, P., and Moore, C.A., *Phys Rev*. **160**, 307-312 (1967).
24. Fonger, W.H., and Struck, C.W., *Phys. Rev. B* **11**, 3251-3260 (1975).